Quantifying the Cellular Uptake of Antibody-Conjugated Au Nanocages by Two-Photon Microscopy and Inductively Coupled Plasma Mass Spectrometry

Leslie Au, Qiang Zhang, Claire M. Cobley, Michael Gidding, Andrea G. Schwartz, Jingyi Chen,* and Younan Xia*

Department of Biomedical Engineering, Washington University, St. Louis, Missouri 63130

ABSTRACT Gold nanocages with localized surface plasmon resonance peaks in the near-infrared region exhibited a broad two-photon photoluminescence band extending from 450 to 650 nm when excited by a Ti:sapphire laser at 800 nm. The bright luminescence makes it possible to explore the use of Au nanocages as a new class of optical imaging agents for two-photon microscopy. In this work, we have demonstrated the use of two-photon microscopy as a convenient tool to directly examine the uptake of antibody-conjugated and PEGylated Au nanocages by U87MGwtEGFR cells. We have also correlated the results from two-photon microscopy with the data obtained by inductively coupled plasma mass spectrometry. Combined together, these results indicate that the antibody-conjugated Au nanocages were attached to the surface of the cells through antibody−antigen binding and then internalized into the cells *via* receptor-mediated endocytosis. The cellular uptake process was dependent on a number of parameters, including incubation time, incubation temperature, size of the Au nanocages, and the number of antibodies immobilized on each nanocage.

KEYWORDS: gold nanostructure · antibody conjugation · cellular uptake · two-photon microscopy · inductively coupled plasma mass spectrometry

Gold nanostructures have recently received increasing interests in biomedical applications due to their spectacular physical and chemical properties, as well as low cytotoxicity.[1] For example, when Au nanostructures interact with an incident light, they can strongly scatter and/or absorb the light at a resonance wavelength depending on the size and shape of the nanostructures. This optical phenomenon has been known as localized surface plasmon resonance (LSPR).[2] When the LSPR peaks are tuned into the near-infrared (NIR) region, particularly, the "transparent window" for soft tissues in the range of 700−900 nm, Au nanostructures can be used as contrast agents for imaging modalities such as optical coherence tomography (OCT) and photoacoustic tomography (PAT).[3−8] They can also be used as nanoscale transducers to convert near-infrared light into heat, providing a new platform for cancer treatment *via* the photothermal effect.[9−12]

Among various Au nanostructures, Au nanocages with hollow interiors and porous walls are of particular interest for biomedical applications because their LSPR peaks can be easily and precisely tuned into the NIR region while maintaining a compact size.[13] Their hollow interiors can also be potentially loaded with various contrast agents and drugs to provide a multifunctional platform for cancer diagnosis and treatment.[14] For such applications to be effective, it is crucial for the Au nanocages to have the capability to selectively target cancer cells rather than healthy ones. Antibodies represent a class of commonly used ligands that can be easily conjugated to the surface of Au nanocages (and other types of nanostructures) for targeting the receptors typically overexpressed on the surface of cancer cells with high specificity. To this end, a quantitative understanding of the cellular uptake of antibody-conjugated Au nanocages *in vitro* can provide valuable information with regard to the design, synthesis, and surface modification of Au nanocages for cancer diagnosis and therapy. It is worth noting that the uptake of nanoparticles by cells depends on not only the size and shape of the particles but also their surface properties.[15] Recent studies show that nanoparticles conjugated with antibodies not only bind to the cell surface *via* the antibody−antigen interaction but also activate membrane receptors and subsequent protein expression.[16]

There are a number of methods for analyzing the uptake of Au nanostructures by cells. One of the commonly used techniques is based upon inductively coupled plasma

*Address correspondence to xia@biomed.wustl.edu, chenj@seas.wustl.edu.

Received for review October 10, 2009 and accepted November 23, 2009.

Published online December 2, 2009.
10.1021/nn901392m

mass spectrometry (ICP-MS), which can measure the concentration of Au ions down to the parts per billion level. This method, however, is rather time-consuming as it requires digestion of the cells containing Au with aqua regia. In contrast, an optical method will provide many advantages. As reported in literature, Au nanostructures can be excited optically, resulting in photoluminescence (PL) emission. The PL emission arose from a recombination of the photoexcited electrons in the s−p conduction band with holes in the d-band of metal surface such as Au, Cu, and Ag.[17,18] This phenomenon is more pronounced for noble metals with feature sizes on the nanometer scale, especially when noble metal nanoparticles were illuminated by a laser in resonance with the LSPR peak.[19−21] The PL can also be induced by two-photon excitation where two low-energy photons were absorbed to excite the electron from d-band to s−p-band of the metal.[18,22] When a Ti:sapphire laser is used, Au nanostructures that have LSPR peak tuned into the NIR region can give strong PL signals under the plasmon-resonant condition. Wang *et al.* have demonstrated that a Au nanorod with a longitudinal LSPR peak at 820 nm could produce PL signals 58 times that of the fluorescence signals from a rhodamine molecule when excited at 820 nm using a two-photon scheme.[23] More recently, Durr *et al.* and Black *et al.* have also shown the use of Au nanorods as contrast agents for two-photon luminescence imaging of cancer cells.[24,25]

Similar to Au nanorods, Au nanocages also have LSPR peaks tunable in the NIR region and are anticipated to emit strong PL when excited using a two-photon scheme under the plasmon-resonant condition. In this work, we examined the two-photon-induced PL of Au nanocages and then used two-photon microscopy to evaluate the uptake of antibody-conjugated Au nanocages by U87MGwtEGFR cells, a cancer cell line that is documented to overexpress epidermal growth factor receptor (EGFR) on the surface. The results were correlated with ICP-MS analysis of Au content to provide a quantitative understanding of the *in vitro* targeting and uptake processes.

RESULTS AND DISCUSSION

We began our studies with Au nanocages having a mean edge length of 50 ± 3 nm and wall thickness of 5 ± 1.2 nm. The monoclonal antibody, anti-EGFR, was conjugated to the surface of Au nanocages using a two-step protocol to generate anti-EGFR Au nanocages. In the first step, *O*-pyridyl disulfide−poly(ethylene glycol)−succinimidyl valeric acid-activated ester (OPSS-PEG-SVA) was attached to the surface of Au nanocages *via* the gold−thiolate chemistry. In the second step, anti-EGFR was coupled to the Au−S−PEG−SVA through an amide bond. The number of anti-EGFR per nanocage could be controlled by adjusting the ratio of anti-EGFR to Au nanocages used for the reaction and quantified using the bicinchoninic acid (BCA) protein assay. Figure 1A displays the extinction spectra of the Au nanocages with a typical TEM image in the inset showing their cubic shape and porous structure. The LSPR peak of the Au nanocages in phosphate buffered saline (PBS) was initially tuned to 770 nm. Surface modification with anti-EGFR red-shifted the LSPR peak by 10 to 780 nm. When the anti-EGFR Au nanocages were transferred into the culture medium, the LSPR peak was further red-shifted to 795 nm due to a change in refractive index for the surrounding medium. The LSPR peak of the anti-EGFR Au nanocages remains symmetric with a Lorentzian shape, indicating that the nanocages were well-dispersed in the culture medium. Differently sized anti-EGFR nanocages were also prepared with their LSPR peaks tuned to 760 and 780 nm (in the culture medium) for nanocages with edge lengths of 35 ± 4 and 90 ± 8 nm, respectively (Figure 1B,C). They exhibited a similar PL profile when excited using a two-photon scheme under the plasmon-resonant condition. Figure 1D shows the typical PL emission spectra from the anti-EGFR Au nanocages as measured using a two-photon microscope. Similar to PL of Au nanorods,[23,25] the Au nanocages exhibited a broad PL band extending from 450 to 650 nm when excited by a Ti:sapphire laser with a peak output at 800 nm. In a control experiment, no PL was observed for an aqueous solution that contained no Au nanocages.

The PL from Au nanocages provides a convenient way to evaluate their *in vitro* targeting capability using two-photon microscopy. In a typical study, U87MGwtEGFR cells were incubated with anti-EGFR Au nanocages for 3 h at 37 °C in the presence of FM4-64 dye, a marker for membrane and endosome. The PL from the Au nanocages was then collected in the range of 500−550 nm, showing a green color (Figure 2A), while the fluorescence from FM4-64 dye was collected in the range of 650−700 nm, exhibiting a red color (Figure 2B). Figure 2C shows superimposition of these two images, indicating that the anti-EGFR Au nanocages were colocalized with the FM4-64 dye. In contrast, cancer cells incubated with the PEGylated Au nanocages under the same condition showed little PL (Figure 2D−F), suggesting that very few PEGylated Au nanocages were attached to or internalized into the cancer cells after 3 h incubation.

When the incubation time was extended to 24 h, the PL intensity originating from the Au nanocages was dramatically enhanced for both anti-EGFR (Figure 3A) and PEGylated Au nanocages (Figure 3B). Note that all of the images were taken with the same setting for PL, so their intensities could be directly compared. We also determined the Au content in the cells by ICP-MS analysis. The concentration of Au was then converted into the number of nanocages using the following equations and plotted in Figure 3C. For a Au nanocage of *L* and *l* in outer and inner edge length, respectively, the number of Au atoms (*n*) containing in each nanocage was determined by

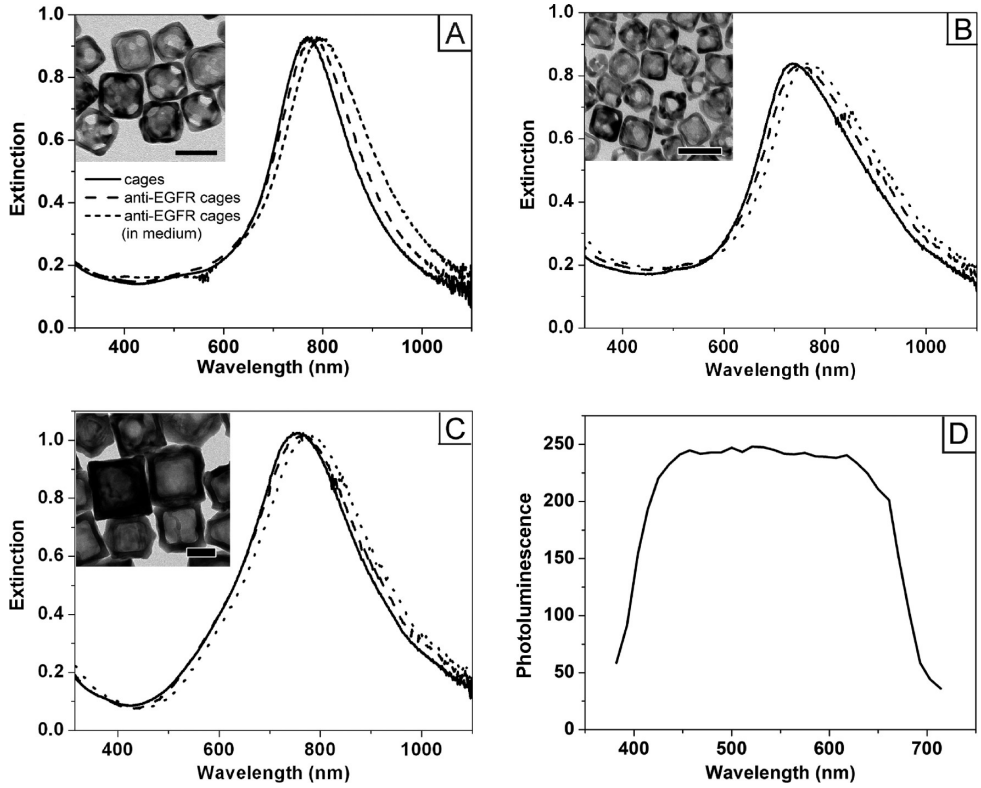

Figure 1. (A−C) UV−vis−NIR extinction spectra of the Au nanocages (solid line) in PBS, anti-EGFR-conjugated Au nanocages (dashed line) in PBS, and anti-EGFR Au nanocages (dotted line) in the culture medium. The insets show TEM images of the corresponding Au nanocages with edge lengths of 50 ± 3, 35 ± 4, and 90 ± 8 nm, respectively. The scale bars in the insets represent 50 nm. (D) Photoluminescence emission spectrum for the Au nanocages of 50 nm in edge length.

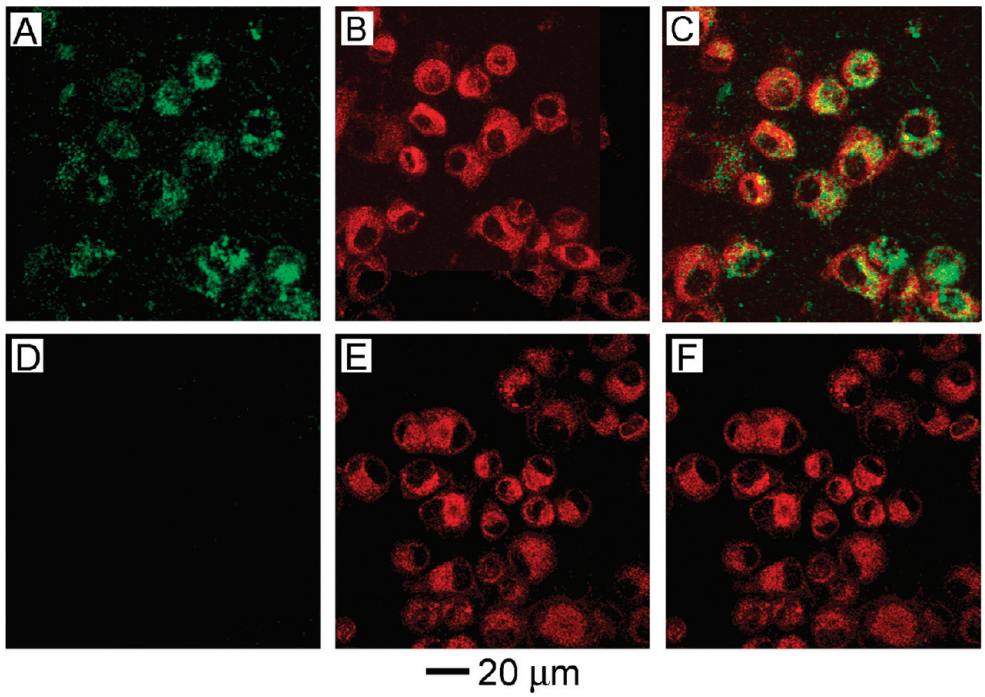

Figure 2. (A−C) Confocal images of the U87MGwtEGFR cells after incubation for 3 h with 0.02 nM of anti-EGFR Au nanocages and 5 μg/mL of FM4-64 dye: (A) photoluminescence from Au nanocages; (B) red fluorescence from FM4-64; and (C) superimposition of (A) and (B). (D,E) Confocal images of the U87MGwtEGFR cells after incubation with PEGylated Au nanocages and FM4-64 dye for 3 h: (D) photoluminescence from Au nanocages; (E) red fluorescence from FM4-64; and (F) superimposition of (D) and (E). The scale bar applies to all images.

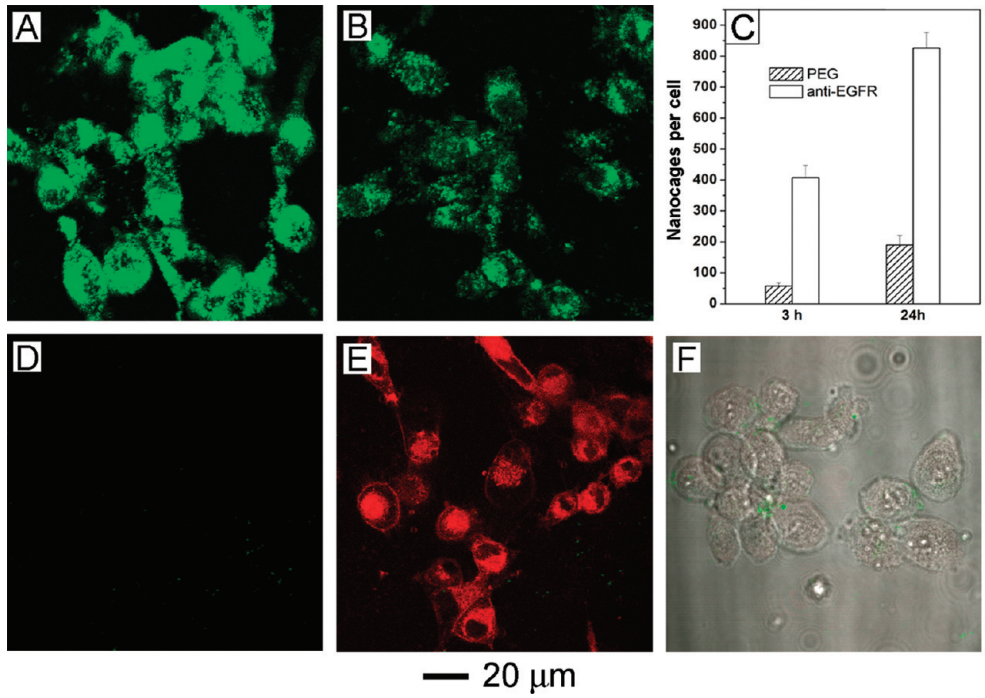

Figure 3. Confocal images of the U87MGwtEGFR cells after they had been incubated for 24 h with (A) anti-EGFR and (B) PEGylated Au nanocages. (C) Quantitative ICP-MS plots showing the number of anti-EGFR and PEGylated Au nanocages per cell for incubation time of 3 and 24 h, respectively. (D−F) Confocal images of the cells that were treated with excess anti-EGFR (100 nM) for 1 h prior to incubation with anti-EGFR nanocages and FM4-64 for 3 h: (D) photoluminescence from Au nanocages and (E) superimposition of the luminescence from Au nanocages and red fluorescence from FM4-64, indicating that the EGF receptors were effectively saturated and there was essentially no uptake for the nanocages. (F) Superimposition of the luminescence from Au nanocages, red fluorescence from FM4-64, and phase contrast image of the cells that were incubated with anti-EGFR nanocages and FM4-64 dye at 4 °C for 1 h. The scale bar applies to all images.

eq 1, where a refers to the lattice constant of a unit cell of Au ($a = 4.08$ Å) and there are four Au atoms per unit cell. The number of Au nanocages (N) can then be calculated by eq 2, where M refers to the measured number of Au ions (atoms) from ICP-MS analysis.

$$n = \frac{4(L^3 - l^3)}{a^3} \quad (1)$$

$$N = \frac{M}{n} \quad (2)$$

At $t = 3$ h, the total number of nanocages taken (including both surface-bounded and internalized) by the cells was 408 ± 40 and 57 ± 10 for anti-EGFR and PEGylated Au nanocages, respectively; these two numbers increased to 826 ± 50 and 190 ± 31 at $t = 24$ h. The overall uptake of the anti-EGFR Au nanocages by the cancer cells was approximately 4−7 times higher than the PEGylated Au nanocages. The high uptake of anti-EGFR Au nanocages can be attributed to the endocytosis mediated by interactions between the anti-EGFR on the surface of nanocage and the receptor overexpressed on the surface of U87MGwtEGFR cells. To further confirm the involvement of receptor-mediated endocytosis (RME) for the anti-EGFR Au nanocages, we treated the cells with excess anti-EGFR to saturate the receptors on the cell surface before incubating them with the anti-EGFR nanocages. Under this condition, no PL was observed for the cells after incubation with the anti-EGFR Au nanocages (Figure 3D). However, the FM4-64 dye was still taken by the cells presaturated with anti-EGFR to display a red color (Figure 3E). These results indicate that the anti-EGFR Au nanocages entered the cells as a result of the interactions between anti-EGFR and its receptor. The uptake of FM4-64 dye likely went through a different internalization pathway that did not work for the Au nanocages. In addition, temperature may affect the binding between anti-EGFR and EGFR, the lateral mobility of the antibody−antigen complex, as well as ATP-dependent process, resulting in inhibition of the RME process.[27,28] When the cells were incubated with anti-EGFR Au nanocages and the FM4-64 dye at 4 °C, neither of them was taken up by the cells (Figure 3F).

The RME process involves the binding of antibodies on the nanoparticles to receptors on the cell surface and internalization of the nanoparticles into the cell when the cell membrane folds inward. Eventually, the receptors may be recycled back to the membrane surface after delivery of the antibody-conjugated nanoparticles into the cell. Differentiation of the internalized particles from the surface-bound particles could shed some light on the RME mechanism and thus enhance the delivery efficacy of antibody-conjugated nanoparticles.[28] After incubation with anti-EGFR Au nanocages, we treated the cells with 20 mM sodium acetate in PBS

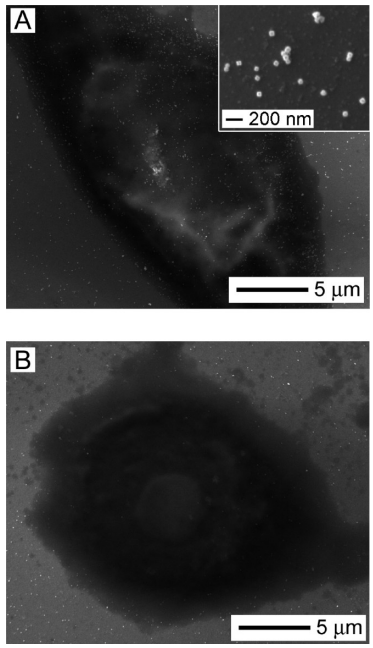

Figure 4. SEM images of the methanol-fixed U87MGwtEGFR cells after incubation with anti-EGFR Au nanocages for 1 h: (A) before and (B) after extensive washing with PBS (pH = 3.0) containing 20 mM sodium acetate, which is supposed to remove the nanocages bound to the cell surface (not the silicon wafer).

(pH = 3.0) buffer. Low pH is one of the commonly used treatments for breaking the antibody−antigen complex. In this case, an acidic solution is expected to selectively release the anti-EGFR Au nanocages bound to the cell surface.[18] Figure 4 shows SEM images of the representative cells before and after the treatment with an acidic solution. Before fixing with methanol, the cells were incubated with anti-EGFR Au nanocages for 1 h at 37 °C, and the excess free nanocages were removed by washing with PBS three times. The membrane of the cell was decorated with hundreds of Au nanocages (Figure 4A). The inset shows a blown-up image of the Au nanocages on the cell membrane. After the treatment with an acidic solution, very few nanocages could be found on the cell surface (Figure 4B), indicating that most of the surface-bound Au nanocages had been selectively removed.

We then studied the cellular uptake of anti-EGFR Au nanocages as a function of incubation time. The U87MGwtEGFR cells were incubated with anti-EGFR nanocages for different periods of time in the culture medium. After removal of the free nanocages from each well, the cells were rinsed with an acidic PBS solution (pH = 3) and the surface-bound nanocages released into the washing solution were collected with a conical tube. The cells were then detached from each well with trypsin and collected with another tube. The washing solution and the trypsinized cells were then digested separately with aqua regia and analyzed for Au content by ICP-MS. Figure 5 shows plots of surface-bound number (N_s), internalized number (N_i), and total

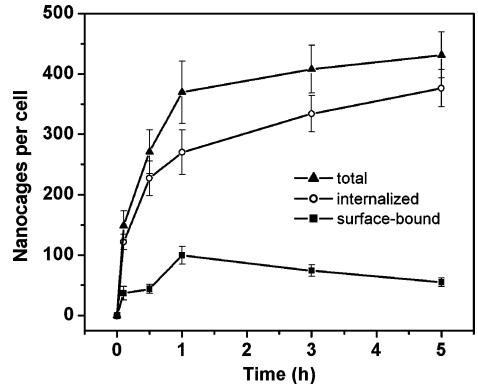

Figure 5. Quantitative ICP-MS analysis of the number of surface-bound (■), internalized (○), and total (▲) anti-EGFR Au nanocages per cell for samples prepared with different incubation time. The surface-bound Au nanocages were selectively detached from the cell surface during the treatment with PBS (pH = 3.0) containing 20 mM of sodium acetate.

number (N_t) of Au nanocages per cell as a function of incubation time. Note that N_s and N_i were derived from the Au concentration measured by ICP-MS, and N_t is simply a sum of N_s and N_i. The N_s initially increased, reached a peak around 1 h, and then fell. The internalization of Au nanocages shows two different profiles: N_i went up sharply in the first 30 min, and the uptake then started to slow down, but still continued to increase up to the end of the study. This finding is different from a previous study with spherical Au nanoparticles. In that case, the uptake was mediated by nonspecific adsorption of serum proteins on the surface of Au nanoparticles, and N_t was significantly increased for the first hour, and then the rate of uptake reached a plateau in the period of 4−7 h.[29] The discrepancy might be due to the difference in terms of receptor availability, ligand−receptor interaction, and the equilibrium condition between the surrounding and interior of the cell.

We also compared the cellular uptake of Au nanocages with different numbers of antibodies on the surface. In this case, the Au nanocages were reacted with anti-EGFR at different molar ratios to obtain samples with roughly 10, 28, and 96 anti-EGFR per nanocage. Figure 6 shows the PL images of the cells after incubation with these anti-EGFR Au nanocages for 3 h and their corresponding superimpositions with confocal images taken from FM4-64 staining. The colocalization of the PL from the Au nanocages and the fluorescence from the FM4-64 confirmed that the nanocages were bound to and/or internalized into the cells. The PL intensity from the cells after treatment with nanocages was enhanced as the number of anti-EGFR per nanocages was increased. This observation was in agreement with the ICP-MS data shown in Figure 7, indicating that the number of Au nanocages per cell increased as the number of anti-EGFR per nanocage increased.

Finally, we compared the internalization of Au nanocages with different sizes. For RME, the uptake rate of

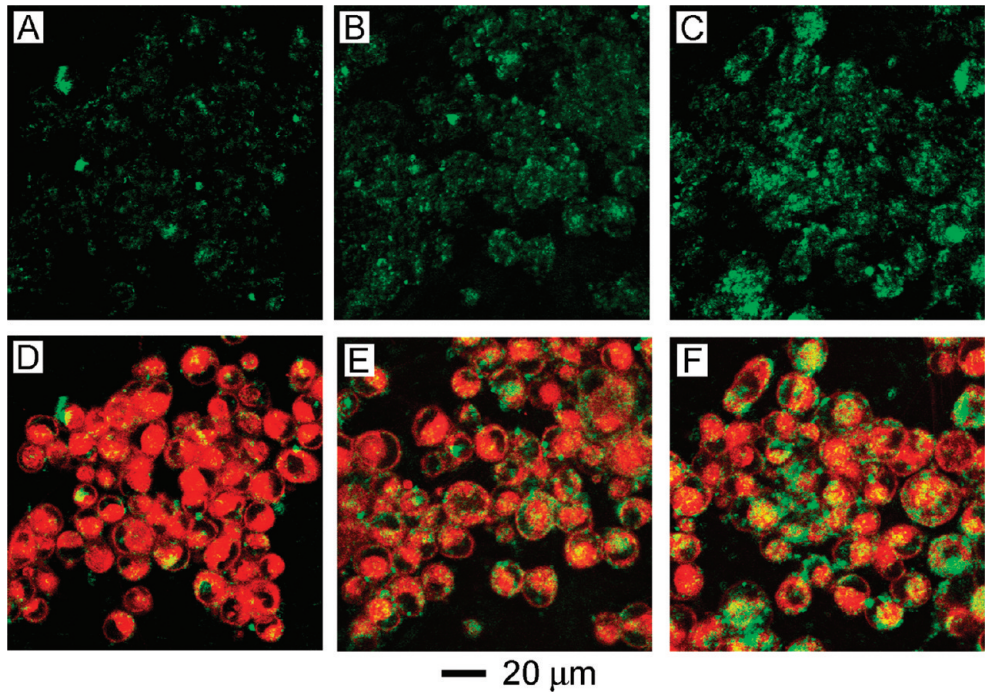

Figure 6. Confocal images of the U87MGwtEGFR cells incubated for 3 h with 5 μg/mL of FM4-64 dye and 0.02 nM of Au nanocages having different numbers of anti-EGFR on the surface. (A−C) Photoluminescence from Au nanocages with roughly (A) 10, (B) 28, and (C) 96 anti-EGFR on the surface of a nanocage, and (D−F) superimpositions of the luminescence from Au nanocages and red fluorescence from FM4-64. The scale bar applies to all images.

particles is size-dependent. Gao *et al.* developed a model involving a wrapping process for the membrane and predicted that the optimum size range for the most efficient wrapping of spherical particles would be in the range of 54−60 nm.[30] From the viewpoint of thermodynamics, Zhang *et al.* also predicted that spherical particles of 50−60 nm in diameter would have a maximum number of uptake into the cell, which was estimated to be in the range of 500−5000.[31] We chose Au nanocages with an edge length of 35 ± 4, 50 ± 3, and 90 ± 8 nm (*i.e.*, Au-35, Au-50, and Au-90) for a comparison study. All of the Au nanocages were conjugated with a maximum number of anti-EGFR per nanocage. By converting the edge length of cubic nanocage into its effective diameter (d_e) with the assumption of equal volume, d_e equals 44, 62, and 112 nm for Au-35, Au-50, and Au-90 nanocages, respectively. Figure 8 shows the number of Au nanocages per cell analyzed by ICP-MS after the cells were incubated with the Au nanocages having different edge lengths. The number of internalized Au nanocages was 605 ± 33, 334 ± 30, and 170 ± 5 for Au-35, Au-50, and Au-90 nanocages, respectively. Clearly, the Au-35 nanocages with d_e of 44 nm were internalized into the cells with the highest number.

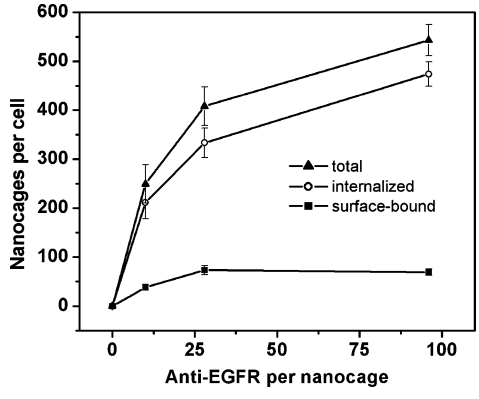

Figure 7. Quantitative ICP-MS analysis of the number of surface-bound (■), internalized (○), and total (▲) anti-EGFR Au nanocages per cell when the cells were incubated for 3 h with 0.02 nM of nanocages having different numbers of anti-EGFR on the surface: 10, 28, and 96. The surface-bound Au nanocages were selectively detached from the cell surface by treating with PBS (pH = 3.0) containing 20 mM of sodium acetate.

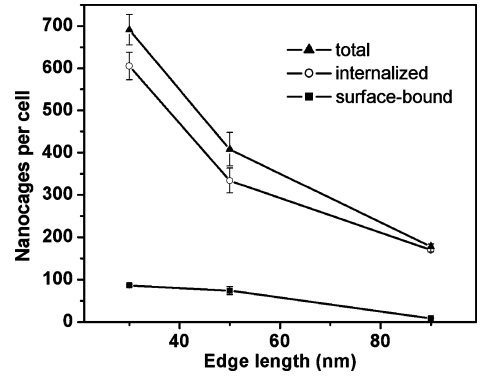

Figure 8. Quantitative ICP-MS analysis of the number of surface-bound (■), internalized (○), and total (▲) anti-EGFR Au nanocages per cell when the cells were incubated for 3 h with 0.02 nM of anti-EGFR Au nanocages with different mean edge lengths: 35, 50, and 90 nm. The surface-bound Au nanocages were detached from the cell surface by treating with PBS (pH = 3.0) containing 20 mM of sodium acetate.

CONCLUSION

We have evaluated the uptake of anti-EGFR Au nanocages by U87MGwtEGFR cancer cells using two-photon microscopy. For Au nanocages with their LSPR peak tuned to 795 nm (in the culture medium), they exhibited a broad luminescence band extending from 450 to 650 nm when excited using a two-photon scheme with a Ti:sapphire laser centered at 800 nm. Two-photon optical images clearly indicate that the anti-EGFR Au nanocages were both attached to the cell surface and internalized into the cell through RME process. The qualitative PL results agree well with the quantitative analysis of Au content by ICP-MS. Our time-dependent study showed a rapid cellular uptake of anti-EGFR nanocages at the beginning. The uptake rate slowed down after the first hour with a total of ~800 anti-EGFR Au nanocages per cell at 24 h. The uptake of Au nanocages increased with the increase in number for anti-EGFR per Au nanocage. The uptake of Au nanocages was also size-dependent, with the 35 nm Au nanocages showing the largest number as compared to 50 and 90 nm samples. The two-photon PL from Au nanocages can be used to quickly screen their interactions with cells, as well as evaluate their distribution in tissue for *ex vivo* and *in vivo* studies.

EXPERIMENTAL METHODS

Chemical and Materials: OPSS-PEG-SVA (*O*-pyridyl disulfide−poly(ethylene glycol)−succinimiyl valeric acid-activated ester, MW ≈ 5000) and mPEG-thiol (methoxy-poly(ethylene glycol)−thiol, MW ≈ 5000) were purchased from Laysan Bio (Arab, AL). Anti-EGFR (monoclonal antibody, clone LA1) was purchased from Millipore (Temecula, CA). The BCA assay kit was purchased from Thermo Scientific (Rockford, IL). The FM4-64 dye, medium DMEM-HG (Dulbecco's modified eagle medium with high glucose), FBS (fetal bovine serum), and G418 (Geneticin) were purchased from Invitrogen (Carlsbad, CA).

Synthesis and Characterization of Au Nanocages: Gold nanocages with mean edge lengths of 35, 50, and 90 nm were synthesized through galvanic replacement by reacting chloroauric acid with Ag nanocubes of 30, 45, and 70 nm in edge length, respectively. The detailed procedure has been reported in our previous publications.[32,33] The LSPR peaks of these nanocages were tuned to 770 nm by controlling the amount of chloroauric acid added into the suspensions of Ag nanocubes. The absorbance spectra were recorded using a Cary 50 UV−vis spectrophotometer (Varian, Palo Alto, CA). TEM samples were prepared by dropping an aqueous suspension of the nanocages onto a carbon-coated copper grid (Ted Pella, Redding, CA) and allowing it to dry under ambient conditions. The sample was continuously rinsed with water for 1 h to remove residual PVP and then dried before TEM characterization. TEM images were collected on a Tecnai G2 Spirit Twin microscope (FEI, Hillsboro, OR) operated at 120 kV. The Au concentrations of the nanocage suspensions were measured using an Agilent 7500ce ICP-MS (Agilent Technologies, Santa Clara, CA). From the ICP-MS data and TEM images, the molar concentrations of the nanocages can be calculated.

Bionconjugation of Au Nanocages: Gold nanocages were functionalized with monoclonal antibodies using a two-step protocol. First, 1 mL of a 1 mM aqueous solution of OPSS-PEG-SVA was mixed with a suspension of Au nanocages 25 pM in concentration. The suspension of nanocages was then agitated for 4 h at room temperature in the dark. After incubation, the solution was centrifuged at 10 000 rpm for 20 min, and the supernatant was removed. The nanocages were washed once with PBS. In the second step, 1 mL of PBS containing 10−120 μg of anti-EGFR was added to the nanocages and incubated at 4 °C for 12 h under agitation. The nanocages were centrifuged down, and the supernatant containing free anti-EGFR was used for BCA assay. The anti-EGFR Au nanocages were redispersed in PBS and stored at 4 °C until future use. For PEGylated samples, the same amount of Au nanocages was mixed with 1 mL of 1 mM mPEG-SH. The solution was agitated for 4 h in the dark at room temperature. Afterward, the solution was centrifuged, washed once with PBS, and redispersed in 1 mL of PBS. The Au contents were analyzed using ICP-MS to determine the final concentration of the functionalized nanocages.

Quantifying the Number of Anti-EGFR per Nanocage: The supernatant collected previously containing unbound anti-EGFR was analyzed using BCA assay. This assay uses a bicinchoninic acid formulation for the colorimetric detection and quantification of protein. The procedures were carried out as provided by the manufacturer. The number of antibodies per nanocage (N_a) was calculated as follows: N_a = the total number of antibodies added − the number of antibodies in the supernatant. Incubation with 10, 35, and 120 μg of anti-EGFR yielded roughly 10, 28, 96 anti-EGFR per Au nanocage, respectively.

Cell Culture: The U87MGwtEGFR cell line was obtained from Prof. Michael J. Welch in the Department of Radiology at Washington University in St. Louis. The cells were cultured in the DMEM-HG supplemented with 10% FBS and 500 mg/L of G418 under 5% CO_2 at 37 °C. The U87MGwtEGFR cells were reseeded 24 h before experiments in a 6-well plate at a population of 5×10^5 cells per well. The medium was changed immediately prior to incubation with Au nanocages. Nanocages (at a final concentration of 0.02 nM) were added into each well and incubated with gentle rotation for a given amount of time as noted in the text. Dye FM4-64, a widely used marker for staining membrane and endosomes, was incubated with the cells simultaneously at a final concentration of 5 μg/mL. After incubation, the cells were rinsed three times with PBS to remove any unbound Au nanocages. For the removal of surface-bound nanocages, the cells were washed for 10 min at 4 °C with 2 mL of a PBS solution containing 20 mM sodium acetate, whose pH had been adjusted to 3.0 with HCl. They were then rinsed again with the 2 mL of PBS solution containing sodium acetate. The washings were collected and saved for ICP-MS analysis. For blocking experiments, anti-EGFR with a final concentration of 100 nM was added to the cells 1 h prior to the addition of nanocages. For experiments at a low temperature, the cells were refrigerated at 4 °C for 10 min prior to and then for 1 h under gentle agitation after the addition of nanocages. The cells were only incubated for 1 h at 4 °C because longer incubation time resulted in cells lifting off from the wells during the washing process.

Two-Photon Confocal Imaging: After washing off the unbound Au nanocages, the cells were covered with a coverslip (#1.5, Corning, Corning, NY) and sealed with vacuum grease. They were kept in the dark and imaged within the next few hours. The imaging was performed using an upright Zeiss LSM 510 NLO system (Carl Zeiss) coupled with a Ti:sapphire laser (Chameleion, Coherent), a green helium−neon (543 nm) laser, and a 63× water immersion objective (Carl Zeiss). The Ti:sapphire laser was operated in a mode-locked configuration at a wavelength overlapping with the LSPR peak of the nanocages, generating sub-200 fs pulse trains at 90 MHz. The PL data were collected using BP500-550IR. The fluorescence dye was excited at 543 nm, and the emission was collected with BP650-700IR. Multi-track mode was used to collect both luminescence and fluorescence images. For comparison, all of the confocal images were taken at the same setting. The emission and excitation spectra of anti-EGFR Au nanocages in PBS were collected using the same microscope. The suspension of nanocages was drawn into a microcapillary tube (Vitrocom, 5002-050) for imaging. For the emission spectrum, the sample was irradiated at 800 nm and the fluorescent images were simultaneously collected at different wavelengths (380−720 nm, 10 nm intervals). The emis-

sion spectrum was derived from the intensity of the fluorescent signal and from the collected images using the Zeiss LSM software.

Sample Preparation for ICP-MS Analysis: For the analysis of surface-bound Au nanocages, the PBS−acetate washings that were previously collected were digested in 5% aqua regia. For internalized nanocages, the cells that had been washed with the acidic PBS solution were removed from the bottom of the well using 2 mL of trypsin, followed by two rinses with 1 mL aliquots of the medium. This solution was collected and then digested with 5% aqua regia. All solutions were centrifuged at 3000 rpm for 5 min to remove any cellular debris which may clog the instrument. The Au contents of the solution were then analyzed using ICP-MS. For each data point in the plot, it was an average from three different samples.

Acknowledgment. This work was supported in part by a Director's Pioneer Award from the NIH (DP1 OD000798) and startup funds from Washington University in St. Louis (to Y.X.), as well as a Pilot Grant from Washington University Molecular Imaging Center supported by NIH (P50 CA94056) (to J.C.). As a visiting student from the University of Science and Technology of China (USTC), Q.Z. was also partially supported by the China Scholarship Council. This work used the facility supported by the Alafi Neuroimaging Laboratory, the Hope Center for Neurological Disorders, and the NIH Neuroscience Blueprint Center Core Grant (P30 NS057105) to Washington University. The authors would like to thank Krys Hyrc and Xenia Meshik for their technical support on the two-photon confocal microscope. Part of the work was performed at the Nano Research Facility (NRF), a member of the National Nanotechnology Infrastructure Network (NNIN), which is supported by the NSF under Award No. ECS-0335765.

REFERENCES AND NOTES

1. Odom, T. W.; Pileni, M.-P. Nanoscience. *Acc. Chem. Res.* **2008**, *41*, 1565–1851.
2. Kreibig, U.; Vollmer, M. *Optical Properties of Metal Cluster*; Springer: Berlin, 1995.
3. Loo, C.; Lin, A.; Hirsch, L.; Lee, M.-H.; Barton, J.; Halas, N.; West, J.; Drezek, R. Nanoshell-Enabled Photonics-Based Imaging and Therapy of Cancer. *Technol. Cancer Res. Treat.* **2004**, *3*, 33–40.
4. Chen, J.; Saeki, F.; Wiley, B. J.; Cang, H.; Cobb, M. J.; Li, Z.-Y.; Au, L.; Zhang, H.; Kimmey, M. B.; Li, X.; Xia, Y. Gold Nanocages: Bioconjugation and Their Potential Use as Optical Imaging Contrast Agents. *Nano Lett.* **2005**, *5*, 473–477.
5. Oldenburg, A. L.; Hansen, M. N.; Zweifel, D. A.; Wei, A.; Boppart, S. A. Plasmon-Resonant Gold Nanorods as Low Backscattering Albedo Contrast Agents for Optical Coherence Tomography. *Opt. Exp.* **2006**, *14*, 6724–6738.
6. Wang, Y.; Xie, X.; Wang, X.; Ku, G.; Gill, K. L.; O'Neal, P.; Stoica, G.; Wang, L. V. Photoacoustic Tomography of a Nanoshell Contrast Agent in the *In Vivo* Rat Brain. *Nano Lett.* **2004**, *4*, 1689–1692.
7. Yang, X.; Skrabalak, S. E.; Li, Z.-Y.; Xia, Y.; Wang, L. V. Photoacoustic Tomography of a Rat Cerebral Cortex *In Vivo* with Au Nanocages as an Optical Contrast Agent. *Nano Lett.* **2007**, *7*, 3798–3802.
8. Song, K. H.; Kim, C.; Cobley, C. M.; Xia, Y.; Wang, L. V. Near-Infrared Gold Nanocages as a New Class of Tracers for Photoacoustic Sentinel Lymph Node Mapping on a Rat Model. *Nano Lett.* **2009**, *9*, 183–188.
9. Hirsch, L. R.; Stafford, R. J.; Bankson, J. A.; Sershen, S. R.; Rivera, B.; Price, R. E.; Hazle, J. D.; Halas, N. J.; West, J. L. Nanoshell-Mediated Near-Infrared Thermal Therapy of Tumors under Magnetic Resonance Guidance. *Proc. Natl. Acad. Sci. U.S.A.* **2003**, *23*, 13549–13554.
10. Huang, X.; El-Sayed, I. H.; Qian, W.; El-Sayed, M. A. Cancer Cell Imaging and Photothermal Therapy in the Near-Infrared Region by Using Gold Nanorods. *J. Am. Chem. Soc.* **2006**, *128*, 2115–2120.
11. Chen, J.; Wang, D.; Xi, J.; Au, L.; Siekkinen, A.; Warsen, A.; Li, Z.-Y.; Zhang, H.; Xia, Y.; Li, X. Immuno Gold Nanocages with Tailored Optical Properties for Targeted Photothermal Destruction of Cancer Cells. *Nano Lett.* **2007**, *7*, 1318–1322.
12. Hasan, W.; Stender, C. L.; Lee, M. H.; Nehl, C. L.; Lee, J.; Odom, T. W. Tailoring the Structure of Nanopyramids for Optimal Heat Generation. *Nano Lett.* **2009**, *9*, 1555–1558.
13. Skrabalak, S. E.; Chen, J.; Sun, Y.; Lu, X.; Au, L.; Cobley, C. M.; Xia, Y. Gold Nanocages: Synthesis, Properties, and Applications. *Acc. Chem. Res.* **2008**, *41*, 1587–1595.
14. Yavuz, M. S.; Cheng, Y.; Chen, J.; Cobley, C. M.; Zhang, Q.; Rycenga, M.; Xie, J.; Kim, C.; Song, K. H.; Schwartz, A. G.; Wang, L. V.; Xia, Y. Gold Nanocages Covered by Small Polymers for Controlled Release with Near-Infrared Light. *Nat. Mater.* DOI: 10.1038/nmat2564.
15. Stellacci, F.; Verma, A. Effect of Surface Properties on Nanoparticle-Cell Interactions. *Small* DOI: 10.1002/smll.200901158.
16. Jiang, W.; Kim, B. Y. S.; Rutka, J. T.; Chan, W. C. W. Nanoparticle-Mediated Cellular Response is Size-Dependent. *Nat. Nanotechnol.* **2008**, *3*, 145–150.
17. Mooradian, A. Photoluminescence of Metals. *Phys. Rev. Lett.* **1969**, *22*, 185–187.
18. Boyd, G. T.; Yu, Z. H.; Shen, Y. R. Photoinduced Luminescence from the Noble Metals and its Enhancement on Roughened Surfaces. *Phys. Rev. B* **1986**, *33*, 7923–7936.
19. Wilcoxon, J. P.; Martin, J. E.; Parsapour, F.; Wiedenman, B.; Kelley, D. F. Photoluminescence from Nanosize Gold Clusters. *J. Chem. Phys.* **1998**, *108*, 9137–9143.
20. Mohamed, M. B.; Volkov, V.; Link, S.; El-Sayed, M. A. The "Lightning" Gold Nanorods: Fluorescence Enhancement of over a Million Compared to the Gold Metal. *Chem. Phys. Lett.* **2000**, *317*, 517–523.
21. Imura, K.; Nagahara, T.; Okamoto, H. Plasmon Mode Imaging of Single Gold Nanorods. *J. Am. Chem. Soc.* **2004**, *126*, 12730–12731.
22. Imura, K.; Nagahara, T.; Okamoto, H. Near-Field Two-Photon-Induced Photoluminescence from Single Gold Nanorods and Imaging of Plasmon Modes. *J. Phys. Chem. B* **2005**, *109*, 13214–13220.
23. Wang, H.; Huff, T. B.; Zweifel, D. A.; He, W.; Low, P. S.; Wei, A.; Cheng, J.-X. *In Vitro* and *In Vivo* Two-Photon Luminescence Imaging of Single Gold Nanorods. *Proc. Natl. Acad. Sci. U.S.A.* **2005**, *102*, 15752–15756.
24. Durr, N. J.; Larson, T.; Smith, D. K.; Korgel, B. A.; Sokolov, K.; Ben-Yakar, A. Two-Photon Luminescence Imaging of Cancer Cells Using Molecularly Targeted Gold Nanorods. *Nano Lett.* **2007**, *7*, 941–945.
25. Black, K. C.; Kirkpatrick, N. D.; Troutman, T. S.; Xu, L.; Vagner, J.; Gillies, R. J.; Barton, J.; Utzinger, U.; Romanowski, M. Gold Nanorods Targeted to Delta Opioid Receptor: Plasmon-Resonant Contrast and Photothermal Agents. *Mol. Imaging* **2008**, *7*, 50–57.
26. Eiblmaier, M.; Meyer, L. A.; Watson, M. A.; Fracasso, P. M.; Pike, L. J.; Anderson, C. J. Correlating EGFR Expression with Receptor-Binding Properties and Internalization of ^{64}Cu-DOTA-Cetuximab in 5 Cervical Cancer Cell Lines. *J. Nucl. Med.* **2008**, *49*, 1472–1479.
27. Pastan, I.; Willingham, M. C. *Endocytosis*. Plenum Press: New York, 1985.
28. Cho, E. C.; Xie, J.; Wurm, P. A.; Xia, Y. Understanding the Role of Surface Charges in Cellular Adsorption versus Internalization by Selectively Removing Gold Nanoparticles on the Cell Surface with a I_2/KI Etchant. *Nano Lett.* **2009**, *9*, 1080–1084.
29. Ruoslahti, E. Antigen−Antibody Interaction, Antibody Affinity, and Dissociation of Immune Complexes. *Scand. J. Immunol.* **1976**, *5*, 3–7.
30. Chithrani, B. D.; Ghazani, A. A.; Chan, W. C. W. Determining the Size and Shape Dependence of Gold Nanoparticle Uptake into Mammalian Cells. *Nano Lett.* **2006**, *6*, 662–668.
31. Gao, H.; Shi, W.; Freund, L. B. Mechanics of Receptor-Mediated Endocytosis. *Proc. Natl. Acad. Sci. U.S.A.* **2005**, *102*, 9469–9474.
32. Sun, Y.; Xia, Y. Mechanistic Study on the Replacement Reaction between Silver Nanostructures and Chloroauric Acid in Aqueous Medium. *J. Am. Chem. Soc.* **2004**, *126*, 3892–3901.
33. Skrabalak, S. E.; Au, L.; Li, X.; Xia, Y. Facile Synthesis of Ag Nanocubes and Au Nanocages. *Nat. Protoc.* **2007**, *2*, 2182–2190.